energies

MDPI

Article

Flexible Yttrium Coordination Geometry Inhibits "Bare-Metal" Guest Interactions in the Metal-Organic Framework Y(btc)

Josie E. Auckett [1,†], Stephen H. Ogilvie [2,†], Samuel G. Duyker [1,2], Peter D. Southon [2], Cameron J. Kepert [2,*] and Vanessa K. Peterson [1,*]

1 Australian Centre for Neutron Scattering, Australian Nuclear Science and Technology Organisation, Lucas Heights, New South Wales 2234, Australia; josiea@ansto.gov.au (J.E.A.); samuel.duyker@sydney.edu.au (S.G.D.)

2 School of Chemistry, The University of Sydney, Sydney, New South Wales 2006, Australia; stephen.ogilvie@sydney.edu.au (S.H.O.); peter.southon@sydney.edu.au (P.D.S.)

* Correspondence: cameron.kepert@sydney.edu.au (C.J.K.); vep@ansto.gov.au (V.K.P.); Tel.: +61-2-9351-5741 (C.J.K.); +61-2-9717-9401 (V.K.P.)

† These authors contributed equally to this work.

Academic Editor: Hai-Wen Li

Received: 31 August 2016; Accepted: 11 October 2016; Published: 18 October 2016

Abstract: Y(btc) (btc = 1,3,5-benzenetricarboxylate) is a metal-organic framework that exhibits significant adsorption of industrially-relevant gases such as H_2, CH_4, and O_2. Previous studies have noted a surprising lack of close interactions between the adsorbed guest molecules and Y, despite the apparent availability of a "bare-metal" binding site. We have extended our previous work in a detailed investigation of the adsorption behaviours of CO_2, CD_4, and O_2 in Y(btc) over a range of concentrations using in situ neutron powder diffraction methods. The O–Y–O bond angles enclosing the bare-metal site are found to change considerably depending on the type and quantity of guest molecules present. Multiple binding sites are found for each guest species, and the largest changes in O–Y–O angles are accompanied by changes in the filling sequences of the binding sites, pointing to an important interplay between guest-induced framework distortions and binding site accessibility. These results suggest the potential for coordinatively flexible rare-earth metal centres to promote guest-selective binding in metal-organic frameworks.

Keywords: adsorption; metal-organic framework; neutron powder diffraction

1. Introduction

The atomic-scale understanding of gas-sorption mechanisms in porous solid sorbents has become a focus of major research efforts in recent times, driven in particular by the need for efficient gas separators in many energy-related applications. Porous crystalline materials such as metal-organic frameworks (MOFs) are often targeted for these applications due to their favourable properties: good gas selectivity and capacity, ease of handling compared to liquid sorbents, as well as adequate mechanical, thermal, and chemical stabilities. Importantly, these materials are highly tuneable, and significant opportunities exist for engineering their chemistries toward particular sorbent applications. Key framework features which improve adsorption properties need to be identified and optimised for the development of better future materials. For example, many studies have shown that the presence of coordinative-unsaturated metal centres tends to enhance total uptake of gases such as hydrogen [1–3], methane [4] and ammonia [5], among others, and can also contribute to guest selectivity in the presence of gas mixtures [6]. These "bare" metal sites interact strongly with many guest molecules, yielding higher binding energies and often resulting in denser arrangements of guests

in the pores of the sorbent material. Unfortunately, the operative stability of bare metal-containing MOFs is often compromised by their ability to readily adsorb guests from the air, such as water and gaseous species, which can lead to permanent degradation of their crystallinity and adsorptive function [7–9]. By contrast, the excellent moisture stability of the well-known $Zr_6O_4(OH)_4(BDC)_6$ (where BDC = benzene-1,4-dicarboxylate), also known as UiO-66(Zr) material, has been partially attributed to the absence of coordinatively unsaturated Zr in the $Zr_6O_4(OH)_4(CO_2)_{12}$ oxide cluster, preventing hydrolytic attack by water molecules [8].

Bare-metal sites are typically created in MOFs by the removal of coordinated solvent molecules from the material following its initial synthesis. In these cases, the preferred coordination geometry of the metal centre and the fixed network topology of the linker molecules both serve to maintain the overall structure of the MOF without significant changes to the framework geometry in the vicinity of the metal centre. However, MOFs containing rare-earth metals may display more flexibility in their coordination geometry upon removal of the solvent due to the greater number of satisfactory geometries adopted by these large metal ions [10–12]. One such example is Y(btc) (btc = 1,3,5-benzenetricarboxylate), a MOF which displays appreciable uptake of H_2 [13], CH_4 and O_2 [14]. Y(btc) is a structural analogue of Tb(btc) (also known as MOF-76 [15]) and consists of parallel 4_1-type helices of Y atoms linked by the bridged carboxylate groups of three btc ligands, resulting in square channels which extend along the *c* axis in the tetragonal space group $P4_322$ (Figure 1). The distance between corresponding atoms on opposite walls of the square channels is ~10.3 Å, equivalent to the *a* parameter of the unit cell. Structural studies have demonstrated significant relaxation of the linker geometry around the Y centre upon removal of the coordinated water-of-crystallisation, yielding a bare-metal site which may be less accessible to guest molecules [14]. In the same study, CD_4 was found to display no significant interaction with the Y centre at 1 CD_4:Y loading, while O_2 interacted weakly with Y only at the least populated of its three observed binding sites. Similarly, no interaction with the bare-metal site was reported for any of the four observed binding locations of D_2 in the material [13].

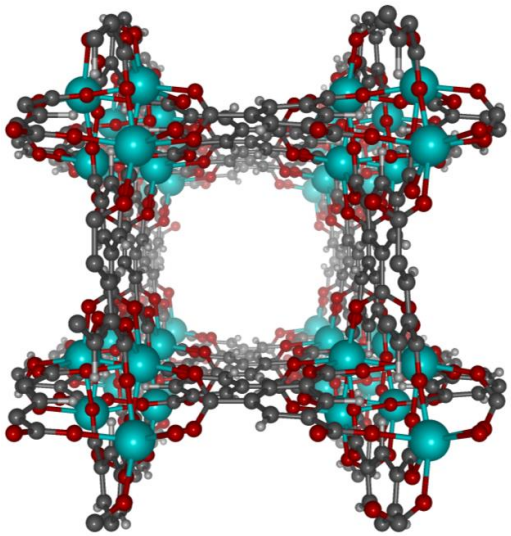

Figure 1. The square channel of Y(btc) viewed along the *c* axis (vanishing perspective is used). Shown are Y (light blue), C (dark grey), O (red) and H (light grey).

The linear CO_2 molecule has a smaller minimum diameter than CH_4 and is more polarisable than either H_2 or O_2, giving it the opportunity for better access to, and more favourable interactions with, the restricted Y bare-metal site in Y(btc). Furthermore, the capture of CO_2 by porous sorbents is of special relevance to the energy industry, due to the drive to minimise carbon dioxide emissions from the waste streams of existing fossil-fuel technologies such as coal plants [16,17], as well as ensuring

the viability of natural gas reserves. We have therefore undertaken a detailed investigation of the adsorption behaviour of CO_2 in Y(btc), extending a previous investigation of CH_4 and O_2 adsorption in the material by exploring the guest concentration effects on both the binding and the framework structure. As with the previous investigations of gas adsorption in Y(btc), neutron scattering methods were used for structural characterisation of the host-guest system, as scattering from the heavy yttrium dominates the X-ray data and inhibits the location of lighter framework and guest atoms. In the context of this new work and of results previously reported for O_2, CH_4, and H_2 [13,14], we present an analysis of the Y coordination environment in Y(btc) and its behaviour in the presence of different guest species and concentrations, with a view to understanding how MOF sorbent functionality is influenced by the use of coordinatively flexible rare-earth metal centres.

2. Results

2.1. Carbon Dioxide Adsorption

2.1.1. Adsorption Isotherms

Gas adsorption isotherms measured for Y(btc) at 298 K demonstrated good uptake of CO_2, the measured value of around 5 mmol·g^{-1} at 10 bar being almost twice the uptake of CH_4 and four times that of O_2 or N_2 at the same pressure and temperature (Figure 2). Uptake kinetics for all gases were very rapid, with equilibration achieved within ~2 min after each dose was applied to the sample. Water adsorption in Y(btc) was found to be fully reversible and the isothermal curve was reproduced after a second adsorption cycle, highlighting the relatively-good stability of the material to moist environments (Figure S1).

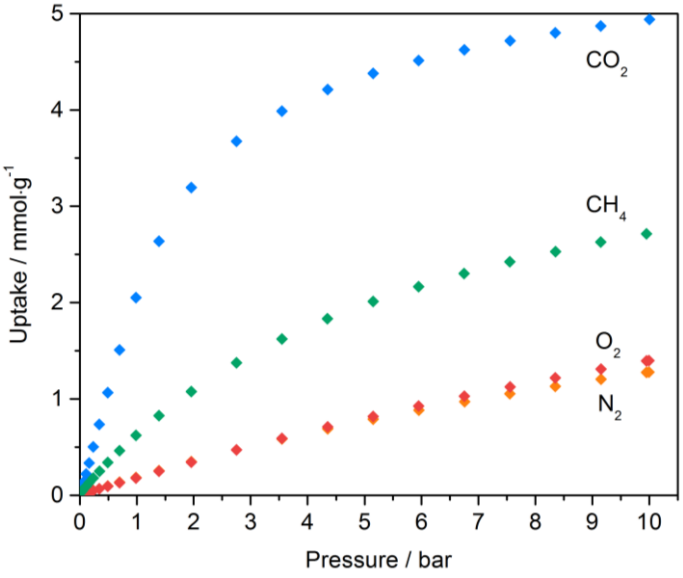

Figure 2. Adsorption isotherms for CO_2, CH_4, O_2 and N_2 at 298 K.

2.1.2. Binding Site Locations

The structure of the empty Y(btc) framework was initially refined against neutron powder diffraction (NPD) data collected for the CO_2-loaded material. Three crystallographically-distinct CO_2 adsorption sites were determined, all of which were observed to be partially occupied after the first dose of 1 CO_2:Y (that is, one mole of CO_2 per mole of Y(btc)) (Table 1). Y(btc)·CO_2 refinement results can be found in the Supporting Information (Tables S1 and S2).

Table 1. Crystallographic details for CO_2 sites within Y(btc) at a dose of 1 CO_2:Y.

Binding Site	Atom	Wyckoff Site	Site Symmetry	Fractional Coordinates			Fractional Occupancy	U_{iso} (10^{-2} Å^2)
				x (*a*)	*y* (*b*)	*z* (*c*)		
A_{CO_2}	C1a	8*d*	1	0.818(4)	0.819(8)	0.359(5)	0.52(2)	21.3(2)
	O1a	8*d*	1	0.831(7)	0.852(7)	0.4347(4)	0.52(2)	21.3(2)
	O1b	8*d*	1	0.853(7)	0.808(8)	0.2850(4)	0.52(2)	21.3(2)
B_{CO_2}	C2a	4*a*	.2.	0.693(1)	0	0.25	0.199(17)	17.5(3)
	O2a	8*d*	1	0.673(8)	0.007(1)	0.1670(2)	0.199(17)	17.5(3)
C_{CO_2}	C3a	4*a*	.2.	0	0.945(1)	0.5	0.111(11)	4.6(2)
	O3a	8*d*	1	0.915(8)	0.950(8)	0.553(1)	0.111(11)	4.6(2)

Figure 3 shows the arrangement and orientation of all symmetry-generated locations for each of the three CO_2 adsorption sites within a single Y(btc) unit cell. The molecules located at sites B_{CO_2} and C_{CO_2} lie along the [y, 0, 1/4] and [0, y, 1/2] 2-fold axes, respectively, and therefore occur with half the multiplicity of site A_{CO_2}. Site occupancy restrictions arising from close interactions between these adsorption sites are discussed in Section 2.1.3.

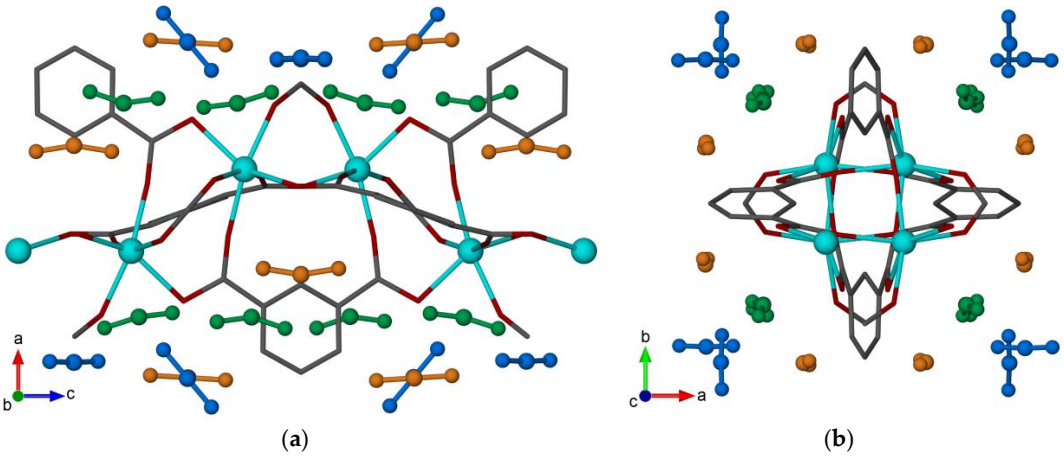

Figure 3. Depiction of all symmetry-generated CO_2 adsorption sites within the Y(btc) unit cell as determined by Rietveld refinement. Adsorption locations are viewed along the (**a**) *b* axis and (**b**) *c* axis. Shown are Site A_{CO_2} (green), Site B_{CO_2} (orange), Site C_{CO_2} (blue), and framework atoms Y (light blue), C (dark grey), and O (red). Framework H atoms are omitted for clarity.

The binding site with the highest CO_2 population, A_{CO_2}, is located approximately 3.1 Å above one carboxylate-functionalised arm of the btc ligand and 4.1 Å from the nearest available bare-metal site. It is interesting to note that one of the shortest host-guest distances is between the A_{CO_2} O atom nearest to the Y bare-metal site and the carboxylate O atom coordinated to the same Y atom. Although electrostatic repulsion is generally expected between two oxygen atoms, it appears likely that the coordinatively unsaturated Y atom draws electron density more strongly from the coordinated atoms, decreasing their partial negative charges to the point where a weak O–O distance of 3.14(10) Å is permitted between them. The other nearest-neighbour distances between A_{CO_2} and Y(btc) are attributed to typical electrostatic interactions between electron-deficient and electron-rich atoms, with observed distances in the intermediate-to-weak range of 2.86–3.42 Å.

The second-most populated CO_2 adsorption site, B_{CO_2}, is located approximately 2 Å above the pseudo-plane of two adjacent btc ligands and interacts symmetrically with four carboxylate functional groups. As a result of the relative positioning and distance from each of these groups, the observed host-guest interactions are attributed to electrostatic interactions dominated by the quadrupolar nature of the CO_2 guest. The O atoms of the CO_2 molecule are positioned 3.17(9) Å from the C atom of the nearest carboxylate group, and 2.94(8) Å from the adjacent C atom on the 6-membered ring.

These electron-deficient C atoms provide a favourable environment with which the electron-rich O guest atoms can interact. Similarly, O atoms from two of the nearby carboxylate groups appear to sandwich the electron-deficient C atom of CO_2, forming a ring of favourable electrostatic host-guest interactions below the guest molecule. Nevertheless, while site B_{CO_2} appears more favourable based on the quantity of electrostatic host-guest interactions, the observed occupancy factor of 0.199(17) CO_2:Y at a loading of 1 CO_2:Y is less than half that of site A_{CO_2}.

The third observed adsorption site, C_{CO_2}, displays the longest host-guest distances and the lowest site occupancies after both CO_2 doses. This site is located 3.628(10) Å and 4.21(3) Å from the nearest and next-nearest btc carboxylate groups, respectively. These distances are generally considered too large to result from significant host-guest interactions, so it is proposed that this site arises from the formation of a bilayer with previously adsorbed CO_2 molecules. When the gas-loaded system is viewed along the *c* axis, it can be seen that site C_{CO_2} is closest to the pore centre (Figure 3b), further supporting this hypothesis.

It should be noted that none of the three CO_2 adsorption sites display any significant interaction with the available Y bare-metal sites, with the closest interaction distances occurring for sites A_{CO_2} and C_{CO_2} at 4.16(9) and 4.640(10) Å, respectively. It is typically expected that the bare-metal sites of a coordination framework should provide guest molecules, particularly quadrupolar CO_2 molecules, with a favourable interaction site. This result will be discussed further below.

The total refined occupancies across the observed CO_2 sites after both doses of CO_2 equated to 80%–85% of the amount of CO_2 dosed, indicating that up to 20% of guests were disordered within the framework and could not be located crystallographically. The relative occupancies of each site remained largely unchanged between the first and second doses, with all occupancy factors increasing by around 100% when the total CO_2 dosage was doubled.

2.1.3. Intermolecular Interactions and Occupancy Restrictions

As seen in Figure 4, several of the possible CO_2 binding sites lie in close proximity to one another, and this is expected to impose some occupancy restrictions. The shortest guest-guest distance of 2.063(1) Å occurs between two symmetrically-equivalent C_{CO_2} sites, restricting the maximum occupancy of this site to 50% (0.5 CO_2:Y). The highest observed C_{CO_2} occupancy factor, ~26%, lies well within this upper bound. The nearest intermolecular distance between sites A_{CO_2} and C_{CO_2} (2.10(8) Å) also restricts the co-occupation of these sites to 50%. As the multiplicity of site A_{CO_2} is 8, the maximum 50% occupancy of this site corresponds to 1 CO_2:Y. This value is approached after the second dose of CO_2.

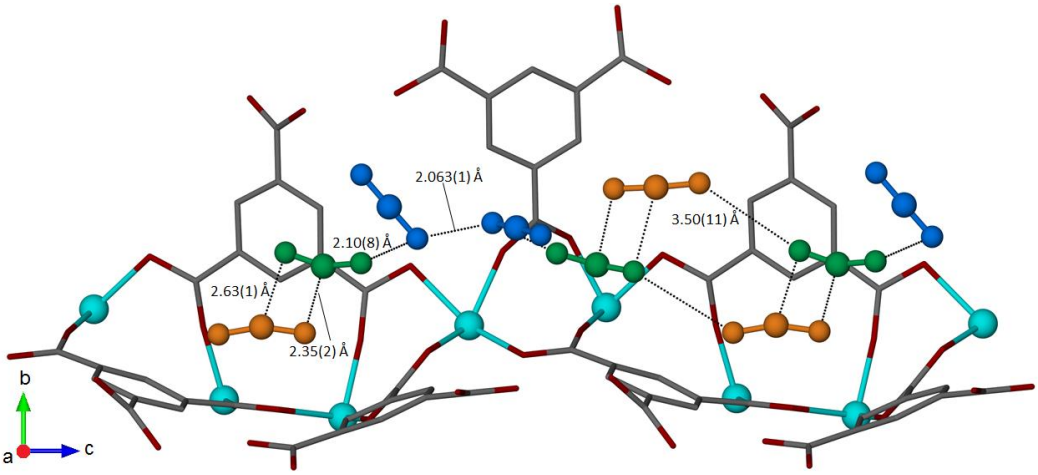

Figure 4. Intermolecular interactions of CO_2 molecules at a dose of 1 CO_2:Y, as viewed along the *a* axis. Shown are CO_2 adsorption-site A_{CO_2} (green), site B_{CO_2} (orange) and site C_{CO_2} (blue), and framework atoms Y (light blue), C (dark grey), and O (red). Framework H atoms are omitted for clarity.

The nearest interactions between sites A_{CO_2} and B_{CO_2} occur at a distance of 2.35(2) Å. These two sites are aligned in an offset-parallel orientation relative to one another that takes advantage of the electrostatic interactions between the slightly positively-charged C and slightly negatively-charged O atoms. Although an end-to-side interaction (similar to that observed in solid CO_2) would more effectively exploit the quadrupolar nature of the CO_2 molecule, the observed arrangement appears to represent an optimal guest-guest configuration given the space constraints inside the Y(btc) pore and the presence of additional host-guest electrostatic interactions.

2.2. Methane and Oxygen Adsorption at High Dosage

Each NPD measurement described in [14] for CD_4 and O_2 at 1 guest:Y dosing was immediately followed by a second dose of 1 guest:Y applied to the same sample, for a total dose amount of 2 guest:Y. NPD data were also collected after the second dose of each gas. The fractional occupancies at all binding sites previously identified for CD_4 and O_2 increased after the second dose, but no new binding sites were identified for either gas (Table 2). Full refinement results for the guest-loaded systems with 2 guest:Y loading can be found in the Supporting Information (Tables S3 and S4).

Table 2. Unit-cell parameters and site-occupancy factors determined using Rietveld analysis of NPD data for empty and guest-loaded Y(btc).

Guest:Y	*a* (Å)	*c* (Å)	Fractional Occupancy				R_{wp} (%)
			Site A	Site B	Site C	Total	
None [1]	10.2998(1)	13.8635(2)	-	-	-	-	3.46
1 CD_4 [1]	10.2970(2)	13.8581(3)	0.39(4)	0.274(8)	-	0.67(5)	4.85
2 CD_4	10.2949(3)	13.8432(4)	0.740(5)	1.006(12)	-	1.75(6)	5.81
1 O_2 [1]	10.2974(3)	13.8600(5)	0.722(16)	0.220(14)	0.198(10)	1.14(4)	5.58
2 O_2	10.29363(15)	13.8522(2)	1.32(2)	0.337(14)	0.440(12)	2.09(5)	3.97
1 CO_2	10.2976(2)	13.8639(3)	0.52(2)	0.199(17)	0.111(11)	0.86(5)	4.85
2 CO_2	10.2709(7)	13.8579(6)	0.966(12)	0.37(2)	0.260(11)	1.59(4)	7.04

[1] From [14].

A reversal of binding site preference upon increased loading was observed for CD_4, with site B_{CD_4} (interacting with the carboxylate groups and first aryl carbon atom) displaying a higher occupancy than site A_{CD_4} (interacting with carboxylate only) after the second dose. Similarly, the preference for guest binding at sites B_{O_2} (near carboxyl and aryl carbons) and C_{O_2} (Y bare metal site) was reversed after the second O_2 dose, though site A_{O_2} (carboxylate groups and first aryl carbon) remained the dominant binding site, containing more than half of the adsorbed O_2.

Adsorption of all guests results in a slight contraction of the unit cell of Y(btc) (Table 2). The *a* parameter decreases slowly and uniformly with increased loading of CO_2, CD_4 and O_2, except for a sharp decrease of ~0.25% between the first and second CO_2 dose. The *c* parameter also decreases uniformly by a similar magnitude, with the largest overall change occurring for O_2 (~0.15% decrease after the second dose).

2.3. The Yttrium Coordination Sphere

The possible region for guest binding between the Y atom and the guest-accessible pore space is enclosed by carboxylate O atoms belonging to four different btc ligands. The opposite pairs of these O atoms are crystallographically equivalent and correspond to sites designated O1 and O3. The angles formed by these atom pairs and the Y centre change considerably upon removal of the water of crystallisation from the as-synthesised framework, with the btc ligands closing in around the vacated binding site (Table 3). The subsequent addition of other guest molecules causes a partial re-opening of the O1–Y–O1 angle, even though the direct interactions between the guests and Y at this location are minimal [14]. Interestingly, the angle opening becomes more pronounced at higher loadings of CD_4 and O_2, but does not change significantly with increased CO_2 loading. The O3–Y–O3

angle, by contrast, contracts further upon the addition of guests to the empty framework. The only exception occurs at the $2O_2$:Y loading where the angle becomes slightly larger than that of the empty framework, probably due to the small amount of O_2 binding to the bare Y site at high loadings [14]. A graphical representation of the changing YO_6 coordination environment is shown in Figure 5.

Table 3. Opposing O–Y–O angles which enclose the bare-metal Y site in the hydrated, dehydrated and guest-loaded Y(btc) materials. O1 and O3 refer to the relevant framework O atoms [13,14].

Guest:Y	O1–Y–O1 (°)	Change from Dehydrated (%)	O3–Y–O3 (°)	Change from Dehydrated (%)
Hydrated	167.9(3)	-	137.6(3)	-
Dehydrated	139.3(5)	-	120.8(5)	-
1 CO_2	143.1(11)	3.8	115.9(8)	−4.9
2 CO_2	143(3)	3.7	115.7(19)	−5.1
1 CD_4	141.9(10)	2.6	114.3(8)	−6.5
2 CD_4	147.2(11)	7.9	114.6(9)	−6.2
1 O_2	141.9(7)	2.6	117.3(6)	−3.5
2 O_2	147.5(8)	8.2	121.4(6)	0.6

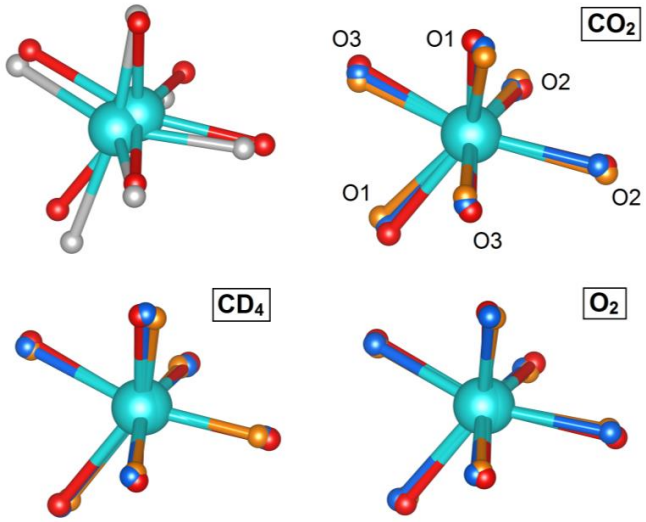

Figure 5. Graphical representation of the YO_6 coordination geometry site in Y(btc) under various guest loading conditions. Y is represented by light blue spheres. The O1, O2 and O3 positions are depicted for the hydrated structure (light grey), empty structure (red), and guest-dosed structures at 1 guest:Y (dark blue) and 2 guest:Y (orange) loading concentrations.

3. Discussion

The four guest species D_2, CO_2, CD_4, and O_2 display markedly different adsorption behaviour in Y(btc). In the absence of direct binding to the bare-metal site, the polar carboxylate groups tend to offer the most favourable adsorption sites and dominate guest occupation at low dosage amounts. However, the precise locations and orientations of these binding sites are unique to each guest, and the order of subsequent site filling also varies among the different species.

D_2 occupies four distinct binding sites, and is the only guest for which these sites are filled in a sequential fashion. Luo et al. [13] found that Site A, which lies near the carboxylate C atoms, is more than 65% occupied before any significant population is observed at Site B, which is closer to the aryl rings. Following the addition of further D_2, Site A saturates and Site C near the carboxylate O atoms populates almost to the level of Site B; B and C then co-fill to saturation. Site D appears to interact primarily with the carboxylate O atoms and other bound D_2 molecules, and is only slightly populated at loadings higher than 4 D_2:Y.

By contrast, CO_2 partially occupies three different binding sites after a single dose of 1 CO_2:Y, though Site A_{CO_2} (near the carboxylate groups) is dominant. All three site populations increase proportionally when the total loading is increased to 2 CO_2:Y. The very similar O–Y–O angles observed after the first and second doses of CO_2 (Table 3) indicate that the framework geometry is not greatly affected by the overall increase in CO_2 loading, which may explain the unchanging relative favourability of the three binding sites.

CD_4 occupies only two binding sites in Y(btc). The population at Site A_{CD_4} is only slightly higher than at Site B_{CD_4} for 1 CD_4:Y, but at higher loadings there is a reversal of preference and Site B_{CD_4} saturates before Site A_{CD_4}. The more rapid increase in the occupancy of B_{CD_4} may indicate that this site is the more energetically favourable adsorption site, but is sterically hindered due to its location in the acute angle between the btc ligands. As additional CD_4 is introduced, the energetic barrier associated with this steric deterrent could be exceeded by guest-guest repulsions, allowing higher occupancy to be achieved. The considerable change in the O1–Y–O1 angle between the first and second doses of CD_4 tends to support the theory that ligand repositioning on increased loading alters the local CD_4 binding environment.

O_2, like CO_2, binds at three different sites which are all partially occupied at 1 O_2:Y loading, with one site dominating strongly. However, the dominant adsorption site A_{O_2} is associated more closely with the carboxylate C and adjoining aryl C atoms than with the carboxylate O atoms favoured by A_{CO_2}. Furthermore, the two less favourable sites (B_{O_2} and C_{O_2}) show a reversal of preference at high loading which is not observed for B_{CO_2} and C_{CO_2}. This is probably due to the very different local environments of the respective sites: C_{O_2} is a bare-metal binding site, whereas the CO_2 molecules at all sites show significant interactions with the ligands only. It is notable that the greatest "opening" of the O–Y–O angles (especially O3–Y–O3) is observed for the second O_2 dose, and this increase in the steric accessibility of the bare Y site is almost certainly linked to the increased favourability of this site at the higher dosing level. A slight decrease of the distance between C_{O_2} and the Y centre from 3.77(6) Å at 1 O_2 to 3.72(4) Å at 2 O_2 is also observed, signifying stronger metal-guest interactions.

Finally, the water adsorption isotherm measured at 298 K (Figure S1) shows a large step, which is also consistent with the initial inaccessibility of the bare Y site. Up to a partial pressure (P_0) of 0.08 the water uptake is comparatively low, and attributed to adsorption only on exterior surface sites. The steep adsorption step, equivalent to approximately 4 water molecules per formula unit, probably occurs when the chemical pressure is sufficient to overcome the energetic barrier to opening the structure.

It is clear that the opening of the O–Y–O angles is important for promoting the accessibility of binding sites which are energetically favourable for otherwise sterically-hindered guest molecules. Whilst O_2 is able to induce this opening at higher concentrations, allowing the guest to interact with the Y, CO_2 is not able to force access to the bare-metal site. Similarly, CD_4 does not interact closely with Y even at high guest loadings, but remains preferentially sandwiched between btc units in a corner position, likely as a consequence of its tetrahedral shape as shown for other MOFs [18].

The demonstrated ability of the btc ligands around Y to undergo guest-specific rearrangement leading to changes in site binding enthalpy has important implications for tailoring sorbent selectivity in MOFs. Guest-induced structural changes are generally common in flexible MOFs [19,20] and can extend even to extreme modifications such as topotactic switching of interpenetration schemes [21], leading to fundamental changes in pore size and shape. Although the effects of the guest-induced site opening in Y(btc) observed in our work are relatively subtle, they represent an avenue for the tuning of adsorptive behaviour which has been largely unexplored so far. The utilisation of these coordinatively flexible metal centres may offer new strategies in MOF design, especially when combined with existing guest-responsive structural features, potentially leading to important applications in carbon capture and fuel storage.

4. Materials and Methods

4.1. Sample Preparation

A mixture of $Y(NO_3)_3 \cdot 6H_2O$ (5.22 g, 13.6 mmol) and 1,3,5-benzenetricarboxylic acid (1.06 g, 5.04 mmol) was dissolved at room temperature in a 1:1:1 (by volume) mixture of N,N-dimethylformamide, ethanol and water (240 mL). This solution was divided equally into four 100 mL Parr Teflon-lined vessels which were heated at a rate of 1.1 $K \cdot min^{-1}$ to 363 K and maintained at this temperature for 18 h. The resulting clear, needle-shaped crystals were allowed to cool to room temperature before being isolated by vacuum filtration and washed with ethanol (100 mL). The combined sample was ground to a fine white powder and desolvated by heating in a glass sample tube at 573 K under high vacuum (~10^{-5} mbar).

4.2. Isothermal Adsorption Measurements

Gas adsorption isotherms for N_2 (supplied at 99.99% purity) and water vapour were measured using the IGA-002 gravimetric system (Hiden-Isochema, Warrington, UK). The freshly-synthesised sample was loaded into a stainless steel basket and heated to 523 K under high vacuum (<10^{-6} mbar) for 7 h, after which the mass (~67 mg) remained stable. Adsorption isotherms were measured at 298 K with the system temperature maintained within 0.1 K. At each data point the pressure in the sample chamber was set and the mass allowed to equilibrate before moving to the next data point. In the case of water isotherms, the maximum equilibration time allowed per pressure point was 5 h, at which point the measurement was continued. The equilibrium mass was corrected for the buoyancy of the sample and balance components.

4.3. Neutron Diffraction

Neutron powder diffraction (NPD) data were collected using the high-resolution neutron powder diffractometer ECHIDNA [22] at the Australian Nuclear Science and Technology Organisation (ANSTO). The desolvated sample (1.376 g) was transferred to a 6 mm-diameter cylindrical vanadium can inside a helium-filled glovebox and loaded onto a custom-designed gas-delivery centrestick, which has been described elsewhere [23,24]. At all times, the sample was maintained *in vacuo* or in a helium atmosphere to prevent unwanted adsorption of gaseous species from the air. The sample stick was inserted into a top-loading cryofurnace for the duration of the experiment, and the sample was repeatedly dosed and reactivated in situ via a thermally-isolated capillary line.

Each dose of a known amount of gas was introduced to the sample at 250 K and slowly cooled to below the condensation/deposition point, at which point the pressure in the system decreased to almost zero. The sample was then cooled over 1 h to the measurement temperature of 10–15 K. No evidence was found any of in the diffraction patterns for the presence of frozen gases, implying that all of the gas was adsorbed by the sample. Diffraction data were acquired over the angular range $17^\circ < 2\theta < 137^\circ$ with an incident neutron wavelength of 2.4425(1) Å, determined using a LaB_6 (NIST SRM 660b) standard reference material. A correction for the Debye-Scherrer ring curvature was applied before data reduction. The sample was re-activated prior to the introduction of new guest species by heating at 350 K under vacuum (~10^{-5} mbar) for approximately 1 h.

4.4. Structural Analysis

Rietveld structural refinements were performed using the program GSAS [25] with the EXPGUI [26] interface. A pseudo-Voigt peak profile function incorporating axial divergence asymmetry (CW neutron Type III, as defined in GSAS) was used, and a 12-term shifted Chebyshev background function was refined. Fractional coordinates and isotropic atomic displacement parameters (ADPs) were refined for all framework atoms. Fourier difference maps were generated in GSAS after initial refinement of the empty framework structure and visualised using VESTA [27] in order to identify

the CO_2 adsorption sites. The CO_2 guests were modelled as complete molecules with variable site occupancies in subsequent refinement cycles.

Supplementary Materials: The following are available online at www.mdpi.com/1996-1073/9/10/836/s1. Figure S1: Water vapour adsorption isotherm for the Y(btc) framework at 298 K. Table S1: Rietveld refinement results for the Y(btc) framework dosed with 1 CO_2:Y. Table S2: Rietveld refinement results for the Y(btc) framework dosed with 2 CO_2:Y. Table S3: Rietveld refinement results for the Y(btc) framework dosed with 2 CD_4:Y. Table S4: Rietveld refinement results for the Y(btc) framework dosed with 2 O_2:Y.

Acknowledgments: This research was supported by the Science and Industry Endowment Fund, the Australian Research Council, and an Australian Institute of Nuclear Science and Engineering Postgraduate Research Award. Research is supported by the Australian Nuclear Science and Technology Organisation's Functional Materials for Energy Systems and Devices project. We thank the sample environment team at the Australian Nuclear Science and Technology Organisation for help with preparing the gas-delivery equipment used in the experiment.

Author Contributions: Stephen H. Ogilvie, Samuel G. Duyker, Josie E. Auckett and Vanessa K. Peterson performed the neutron experiments and analyses; Stephen H. Ogilvie, Peter D. Southon and Cameron J. Kepert performed the chemical syntheses and analyses; Josie E. Auckett wrote the paper with input from all authors.

Conflicts of Interest: The authors declare no conflict of interest.

References

1. Liu, Y.; Kabbour, H.; Brown, C.M.; Neumann, D.A.; Ahn, C.C. Increasing the Density of Adsorbed Hydrogen with Coordinatively Unsaturated Metal Centers in Metal-Organic Frameworks. *Langmuir* **2008**, *24*, 4772–4777. [CrossRef] [PubMed]
2. Yang, Q.; Zhong, C. Understanding Hydrogen Adsorption in Metal-Organic Frameworks with Open Metal Sites: A Computational Study. *J. Phys. Chem. B* **2006**, *110*, 655–658. [CrossRef] [PubMed]
3. Rowsell, J.L.C.; Yaghi, O.M. Effects of Functionalization, Catenation, and Variation of the Metal Oxide and Organic Linking Units on the Low-Pressure Hydrogen Adsorption Properties of Metal-Organic Frameworks. *J. Am. Chem. Soc.* **2006**, *128*, 1304–1315. [CrossRef] [PubMed]
4. Wu, H.; Zhou, W.; Yildirim, T. High-Capacity Methane Storage in Metal-Organic Frameworks M-2(dhtp): The Important Role of Open Metal Sites. *J. Am. Chem. Soc.* **2009**, *131*, 4995–5000. [CrossRef] [PubMed]
5. Rieth, A.J.; Tulchinsky, Y.; Dincă, M. High and Reversible Ammonia Uptake in Mesoporous Azolate Metal-Organic Frameworks with Open Mn, Co, and Ni Sites. *J. Am. Chem. Soc.* **2016**, *138*, 9401–9404. [CrossRef] [PubMed]
6. Karra, J.R.; Walton, K.S. Effect of Open Metal Sites on Adsorption of Polar and Nonpolar Molecules in Metal-Organic Framework Cu-BTC. *Langmuir* **2008**, *24*, 8620–8626. [CrossRef] [PubMed]
7. Ming, Y.; Purewal, J.; Yang, J.; Xu, C.C.; Soltis, R.; Warner, J.; Veenstra, M.; Gaab, M.; Muller, U.; Siegel, D.J. Kinetic Stability of MOF-5 in Humid Environments: Impact of Powder Densification, Humidity Level, and Exposure Time. *Langmuir* **2015**, *31*, 4988–4995. [CrossRef] [PubMed]
8. DeCoste, J.B.; Peterson, G.W.; Schindler, B.J.; Killops, K.L.; Browe, M.A.; Mahle, J.J. The effect of water adsorption on the structure of the carboxylate containing metal-organic frameworks Cu-BTC, Mg-MOF-74, and UiO-66. *J. Mater. Chem. A* **2013**, *1*, 11922–11932. [CrossRef]
9. Singh, M.P.; Dhumal, N.R.; Kim, H.J.; Kiefer, J.; Anderson, J.A. Influence of Water on the Chemistry and Structure of the Metal Organic Framework Cu-3(btc)(2). *J. Phys. Chem. C* **2016**, *120*, 17323–17333. [CrossRef]
10. Duyker, S.G.; Halder, G.J.; Southon, P.D.; Price, D.J.; Edwards, A.J.; Peterson, V.K.; Kepert, C.J. Topotactic structural conversion and hydration-dependent thermal expansion in robust $LnM^{III}(CN)_6{\cdot}nH_2O$ and flexible $ALnFe^{II}(CN)_6{\cdot}nH_2O$ frameworks (A = Li, Na, K; Ln = La–Lu, Y; M = Co, Fe; $0 \leq n \leq 5$). *Chem. Sci.* **2014**, *5*, 3409–3417. [CrossRef]
11. Duyker, S.G.; Peterson, V.K.; Kearley, G.J.; Ramirez-Cuesta, A.J.; Kepert, C.J. Negative Thermal Expansion in $LnCo(CN)_6$ (Ln=La, Pr, Sm, Ho, Lu, Y): Mechanisms and Compositional Trends. *Angew. Chem. Int. Ed.* **2013**, *52*, 5266–5270. [CrossRef] [PubMed]
12. Duyker, S.G.; Peterson, V.K.; Kearley, G.J.; Studer, A.J.; Kepert, C.J. Extreme compressibility in $LnFe(CN)_6$ coordination framework materials via molecular gears and torsion springs. *Nat. Chem.* **2016**, *8*, 270–275. [CrossRef] [PubMed]

13. Luo, J.; Xu, H.; Liu, Y.; Zhao, Y.; Daemen, L.L.; Brown, C.; Timofeeva, T.V.; Ma, S.; Zhou, H.C. Hydrogen Adsorption in a Highly Stable Porous Rare-Earth Metal-Organic Framework: Sorption Properties and Neutron Diffraction Studies. *J. Am. Chem. Soc.* **2008**, *130*, 9626–9627. [CrossRef] [PubMed]
14. Ogilvie, S.H.; Duyker, S.G.; Southon, P.D.; Peterson, V.K.; Kepert, C.J. Host-guest adsorption behavior of deuterated methane and molecular oxygen in a porous rare-earth metal-organic framework. *Powder Diffr.* **2014**, *29*, S96–S101. [CrossRef]
15. Rosi, N.L.; Kim, J.; Eddaoudi, M.; Chen, B.L.; O'Keeffe, M.; Yaghi, O.M. Rod packings and metal-organic frameworks constructed from rod-shaped secondary building units. *J. Am. Chem. Soc.* **2005**, *127*, 1504–1518. [CrossRef] [PubMed]
16. D'Alessandro, D.M.; Smit, B.; Long, J.R. Carbon Dioxide Capture: Prospects for New Materials. *Angew. Chem. Int. Ed.* **2010**, *49*, 6058–6082. [CrossRef] [PubMed]
17. Sumida, K.; Rogow, D.L.; Mason, J.A.; McDonald, T.M.; Bloch, E.D.; Herm, Z.R.; Bae, T.-H.; Long, J.R. Carbon Dioxide Capture in Metal-Organic Frameworks. *Chem. Rev.* **2012**, *112*, 724–781. [CrossRef] [PubMed]
18. Wu, H.; Simmons, J.M.; Liu, Y.; Brown, C.M.; Wang, X.-S.; Ma, S.; Peterson, V.K.; Southon, P.D.; Kepert, C.J.; Zhou, H.C.; et al. Metal-Organic Frameworks with Exceptionally High Methane Uptake: Where and How is Methane Stored? *Chem. Eur. J.* **2010**, *16*, 5205–5214. [CrossRef] [PubMed]
19. Li, A.; Li, L.; Lin, Z.; Song, L.; Wang, Z.H.; Chen, Q.; Yang, T.; Zhou, X.H.; Xiao, H.P.; Yin, X.J. Guest-induced reversible structural transitions and concomitant on/off luminescence switching of an Eu(III) metal-organic framework and its application in detecting picric acid. *New J. Chem.* **2015**, *39*, 2289–2295. [CrossRef]
20. Li, J.R.; Kuppler, R.J.; Zhou, H.C. Selective gas adsorption and separation in metal-organic frameworks. *Chem. Soc. Rev.* **2009**, *38*, 1477–1504. [CrossRef] [PubMed]
21. Chen, Q.; Chang, Z.; Song, W.C.; Song, H.; Song, H.B.; Hu, T.L.; Bu, X.H. A Controllable Gate Effect in Cobalt (II) Organic Frameworks by Reversible Structure Transformations. *Angew. Chem. Int. Ed.* **2013**, *52*, 11550–11553. [CrossRef] [PubMed]
22. Liss, K.D.; Hunter, B.; Hagen, M.; Noakes, T.; Kennedy, S. Echidna—the new high-resolution powder diffractometer being built at OPAL. *Phys. B Condens. Matter* **2006**, *385*, 1010–1012. [CrossRef]
23. Chevreau, H.; Duyker, S.G.; Peterson, V.K. Using neutron powder diffraction and first-principles calculations to understand the working mechanisms of porous coordination polymer sorbents. *Acta Crystallogr. Sect. B* **2015**, *71*, 648–660. [CrossRef] [PubMed]
24. Lee, S.; Chevreau, H.; Booth, N.; Duyker, S.G.; Ogilvie, S.H.; Imperia, P.; Peterson, V.K. Powder sample-positioning system for neutron scattering allowing gas delivery in top-loading cryofurnaces. *J. Appl. Crystallogr.* **2016**, *49*, 705–711. [CrossRef]
25. Larson, A.C.; Von Dreele, R.B. *General Structural Analysis System (GSAS)*; LAUR 86-748; Los Alamos National Laboratory Report: Los Alamos, NM, USA, 2000.
26. Toby, B.H. EXPGUI, a graphical user interface for GSAS. *J. Appl. Crystallogr.* **2001**, *34*, 210–213. [CrossRef]
27. Momma, K.; Izuma, F. VESTA: A three-dimensional visualization system for electronic and structural analysis. *J. Appl. Crystallogr.* **2008**, *41*, 653–658. [CrossRef]